Inclusive Λ^0 production by 12-GeV protons on nuclear targets

F. Abe, K. Hara, N. Kim, K. Kondo, S. Miyashita, H. Miyata, I. Nakano, T. Sugaya, K. Takikawa, R. Tanaka,* Y. Yamamoto, T. Yasuda,† and K. Yasuoka‡
Institute of Physics, University of Tsukuba, Sakura, Niihari, Ibaraki 305, Japan

Y. Asano, Y. Iguchi, and S. Mori
Institute of Applied Physics, University of Tsukuba, Sakura, Niihari, Ibaraki 305, Japan

Y. Fukui, S. Kurokawa, and A. Maki
National Laboratory for High Energy Physics (KEK), Oho, Tsukuba, Ibaraki 305, Japan
(Received 26 June 1984)

The invariant cross sections for inclusive Λ^0 production by 12-GeV protons on nuclei have been measured for three nuclear targets, beryllium, copper, and tungsten. Data are obtained at three production angles of 3.5°, 6.5°, and 9.5° in the laboratory, which cover the kinematic range $0.2 \leq x_F \leq 0.9$ and $0.35 \leq p_T \leq 1.7$ GeV/c. The present results are compared with other work at higher energies in terms of the A dependence, Feynman scaling, the p_T distribution, and triple-Regge behavior.

I. INTRODUCTION

Measurements of inclusive Λ^0 production by high-energy protons were mostly made with bubble chambers until recently.[1] These experiments provided data on the cross sections over a wide kinematic range. However, the statistics of the data were limited, and the results were usually presented as cross sections integrated over one of the kinematic variables. The recent development[2,3] of the Λ^0 beam produced in proton-nucleus collisions allowed the accumulation of high-statistics data and also the study of the dependence of production cross sections on the atomic mass of the target nucleus (the A dependence).

A Λ^0 beam line[4] was constructed at KEK by using the slow-extracted primary proton beam of the 12-GeV proton synchrotron. The KEK Λ^0 beam was exploited to study inclusive Λ^0 production in proton-nucleus collisions at the energy region of 12 GeV. In this paper we present the invariant cross sections for inclusive Λ^0 production on three target materials, beryllium (Be), copper (Cu), and tungsten (W). Data were obtained at three production angles of 3.5°, 6.5°, and 9.5° in the laboratory. In terms of the Feynman scaling variable x_F and the transverse momentum p_T of the produced Λ^0, the kinematic range covered is $0.2 \leq x_F \leq 0.9$ and $0.35 \leq p_T \leq 1.7$ GeV/c. The polarization of Λ^0's from the tungsten target, which was measured prior to this experiment, was already reported.[5]

The A dependence of hadron-production cross sections is of current interest in high-energy physics, because the interactions of high-energy particles with nuclear targets are expected to provide a unique opportunity to study the space-time development of hadron-production processes.[6] Experimental data on the A dependence of Λ^0 production in proton-nucleus collisions is scarce and comes solely from the Fermilab experiment[2] at 300 GeV. The production of Λ^0's in proton-nucleus collisions is a reaction suitable to study the hadron-production process, since it involves the creation of a new quark flavor (s quark). In fact, the work of Ref. 2 stimulated several theoretical models[7,8] of hadron-nucleus collisions in terms of quark-parton pictures. The present experiment provides new data on the A dependence of Λ^0 production at the energy region of 12 GeV.

The present results will also be discussed in terms of Feynman scaling and triple-Regge behavior. Feynman scaling[9] is a well-known phenomenon in high-energy inclusive reactions. The scaling law predicts that the invariant cross section as a function of x_F and p_T does not depend on the incident energy at the high-energy limit. The scaling property for charged-particle production in proton-proton collisions has been studied extensively.[1,10] On the other hand, the scaling property for Λ^0 production has been studied[1] exclusively in terms of cross sections integrated over p_T. The results so far obtained seem to indicate that the scaling limit is approached from below and is reached at an incident proton energy greater than ~ 30 GeV.[1] Comparison of our data with the results[2] at 300 GeV as a function of (x_F, p_T) permits a test of Feynman scaling for Λ^0 production.

The triple-Regge model[11] gives a useful phenomenological description of high-energy inclusive reactions.[12] Triple-Regge analyses of Λ^0 production by proton beams were performed by Blobel *et al.*[13] at 12 and 24 GeV/c, by Alpgård *et al.*[14] at 19 GeV/c, by Blumenfeld *et al.*[15] at 69 GeV/c, and by Devlin *et al.*[16] at 300 GeV. Although these data are well reproduced by the triple-Regge model, the Regge trajectory $\alpha_R(t)$ obtained in Ref. 16 is significantly different from that obtained in other experiments. The triple-Regge analysis of our data is useful to elucidate the discrepancies observed among the previous experiments.

We describe the experimental apparatus and procedures in Sec. II. The data reduction is described in Sec. III. Our results of the invariant cross sections are presented in comparison with other experiments in Sec. IV. The conclusions are summarized in Sec. V.

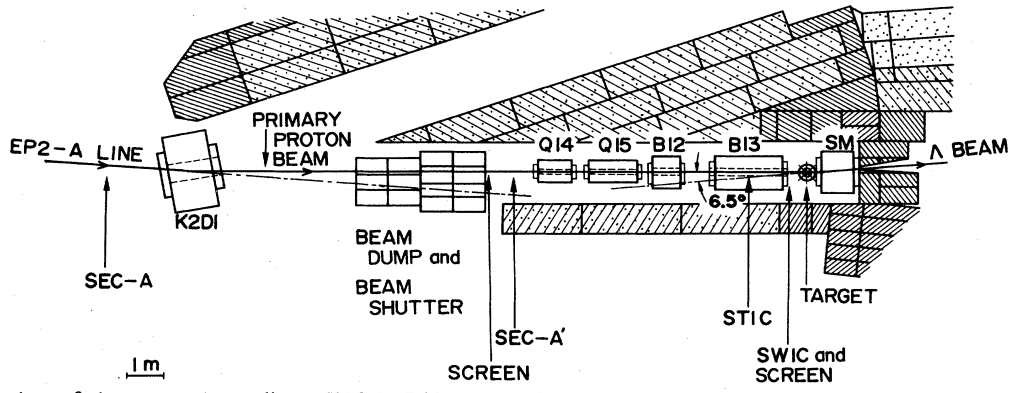

FIG. 1. Top view of the proton beam line. $K2D1$, $B12$, and $B13$ are bending magnets; $Q14$ and $Q15$ are quadrupole magnets; SEC-A and SEC-A' are secondary-emission chambers; STIC is a split transverse ion chamber, which monitors the horizontal beam position at the center of $B13$ (Ref. 4); SWIC is a segmented-wire ion chamber; SCREEN's are fluorescent screens.

II. EXPERIMENTAL APPARATUS AND PROCEDURES

The experimental apparatus was already described in previous publications.[4,5] In this paper we briefly describe the apparatus with an emphasis on those aspects which are immediately relevant to the present measurement of the Λ^0 production cross sections.

Figure 1 illustrates a top view of the proton beam line used in this experiment. The proton beam line was at an angle of 6.5° with respect to the Λ^0 detection system. The Λ^0 production angles of 3.5° and 9.5° were obtained by deflecting the proton beam horizontally and restoring it to the target with two steering magnets ($B12$ and $B13$). The proton beam was focused on the target by two quadrupole magnets ($Q14$ and $Q15$). The beam size at the position of the target was 6 mm (full width at half maximum) both horizontally and vertically. The intensity of the proton beam was monitored by two secondary emission chambers (SEC-A and SEC-A').[17] The beam intensity was approximately 1×10^{10} protons per pulse at 9.5°, and 3×10^{9} protons per pulse at 3.5° and 6.5°.

The target materials used in this experiment were beryllium ($A=9.01$), copper ($A=63.54$), and tungsten ($A=183.85$). The physical dimension of the targets used for data taking was 30 mm wide, 10 mm high, and 20 mm thick for each of the three target materials. Targets twice as thick as the above three were used to measure the absorption effects in the targets. In addition, a large plate of copper, 100 mm wide, 100 mm high, and 20 mm thick, was used to determine the fractional number of the beam protons that struck the target.

A neutral beam was defined by a 1.2-m-long brass collimator placed in the vertical magnetic field of a sweep magnet (SM). The collimator had a tapered rectangular hole, 13 mm wide × 11 mm high at the entrance and 15 mm × 15 mm at the exit. The solid angle of acceptance was defined to be 100 μsr at the exit of the collimator.

The Λ^0's were identified by detecting the proton and the pion from the $\Lambda^0\to p\pi^-$ decay. Figure 2 shows a schematic diagram of the Λ^0 detection system. The system consisted of two spectrometer magnets ($D1$ and $D2$), 24 planes of wire chambers, and five trigger counters. The magnet $D1$ was a large-aperture spectrometer magnet to measure the π^- momentum, while $D2$ was a high-analyzing power magnet to measure the proton momentum. Particle trajectories were determined by multiwire proportional chambers (PC1 and PC2) and multiwire drift chambers (DC1 to DC4). Each chamber had four signal planes of X (horizontal), Y (vertical), U (inclined at 45° with respect to X), and V (inclined at 135° with respect to X). Scintillation counters ($S1$ to $S5$) were used for the event trigger. The $S1$ defined the upstream end of the decay region for the $\Lambda^0\to p\pi^-$ decay, and $S2$ its downstream end. The distance of $S1$ from the production target was 2.17 m, which corresponded to 3.8 times the mean flight path of Λ^0's of 8 GeV/c, the average momentum of Λ^0's in this experiment. The counters $S2$ to $S5$ were placed so as to detect the decay protons from the Λ^0 decay. The event trigger was generated when a high-momentum particle hit $S2$ through $S5$ in the absence of the signal from $S1$.

For the readout electronics of the proportional chambers we used a serial data-transfer system of the Yale-Tsukuba type.[18] The drift chambers were read out with a conventional system consisting of the LeCroy DC201A discriminator and 2770A digitizer. A mini-

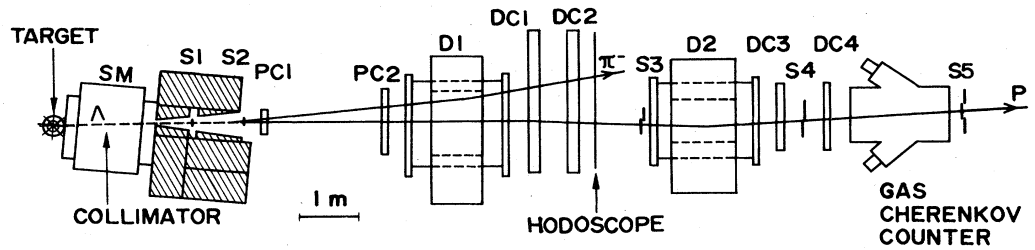

FIG. 2. Top view of the Λ^0 detection system. A typical $\Lambda^0\to p\pi^-$ event is illustrated.

TABLE I. The measured number of $\Lambda^0 \to p\pi^-$ events. The ratio of the number of reconstructed $\Lambda^0 \to p\pi^-$ events to that of the triggers is shown in parentheses.

Target material	Target thickness (mm)	Target thickness (g/cm^2)	Number of events $\theta=3.5°$	Number of events $\theta=6.5°$	Number of events $\theta=9.5°$
Be	20	3.70	9940 (6.4%)	8240 (5.2%)	1650 (1.8%)
	40	7.39		2960 (5.8%)	
Cu	20	17.9	15500 (9.8%)	17900 (7.8%)	2600 (3.1%)
	40	35.8		11000 (9.4%)	
W	20	38.6	13900 (11.5%)	11200 (10.9%)	2860 (4.6%)
	40	77.2		11500 (13.6%)	

data-processor Eclipse S/230 associated with a CAMAC branch highway formed the core of the data-acquisition system.

During the data-taking runs at each production angle, the three 20-mm-thick targets were cyclically interchanged to reduce the target-to-target errors. When switching from one angle to another, we made the copper-target runs at the two angles alternately several times to reduce the angle-to-angle errors. The data for the 40-mm-thick targets were collected at 6.5°. The empty target runs were made at each angle.

The absolute intensity calibration of the proton beam was made with the help of the activation method of aluminum foil, which was based on the known cross section[19] for the $^{27}Al(p,3pn)^{24}Na$ reaction at 12 GeV. The activity of ^{24}Na was measured by detecting the 1368.5-keV γ rays with a germanium detector. The detection efficiency of the germanium detector was measured with standard ^{60}Co checking sources. The overall uncertainty in the beam-intensity calibration[4] was 15%.

III. DATA REDUCTION

The data reduction in this experiment can be divided into four parts: (1) track finding and kinematic reconstruction of $\Lambda^0 \to p\pi^-$ events, (2) Monte Carlo calculation of the detector acceptance, (3) calculation of the invariant cross sections, and (4) corrections.

A. Track finding and kinematic reconstruction

The kinematics of the $\Lambda^0 \to p\pi^-$ decay has the following characteristics. The positively charged (proton) track makes a small angle with respect to the parent Λ^0 direction, carrying most of the Λ^0 momentum. The negatively charged (pion) track spreads over larger angles with respect to the Λ^0 direction, with relatively lower momenta. They form a vertex within the decay region (neutral-vee events). We took advantage of these features in the track-finding program, the details of which were described elsewhere.[5]

Neutral-vee events selected in the track finding were then processed by the kinematic reconstruction program. The decay point and the momentum vector of the parent particle were calculated from two trajectories of opposite charges. The decay point was defined by a vertex point having the closest distance between the two trajectories. The parent particle was traced to the exit of the collimator and back to the target, where the geometrical cuts were applied. About 15% of the vee events were rejected by these cuts. In order to remove the $\gamma \to e^+e^-$ contamination, the invariant mass was formed under the hypothesis that a negatively charged particle was an electron and a positively charged one was a positron. About 10% of the vee events turned out to be γ's. The final selection of $\Lambda^0 \to p\pi^-$ events was based on the distribution of the $p\pi^-$ invariant mass. The mass spectrum had an approximately uniform background of 2% under the Λ^0 mass peak. The background was probably due to errors in the track finding and also to the $K_S^0 \to \pi^+\pi^-$ contamination, and was subtracted at each bin of the Λ^0 momentum. The number of $\Lambda^0 \to p\pi^-$ events finally accepted is listed in Table I.

The Λ^0 yield in the empty-target runs was at most 5% of the target-in yield. The empty-target background was subtracted at each bin of the Λ^0 momentum.

B. Monte Carlo calculation of the detector acceptance

The efficiency of the present spectrometer to detect Λ^0's was calculated with a Monte Carlo method. A sample of Λ^0's was generated at the target, with a spatial distribution consistent with the proton beam profile, and with the direction of motion in an appropriate interval of angles. The Λ^0's were traced through the collimator to the decay region, where they were allowed to decay into the proton and the π^-, which in turn were traced through the spectrometer. The tracing of the proton and the π^-

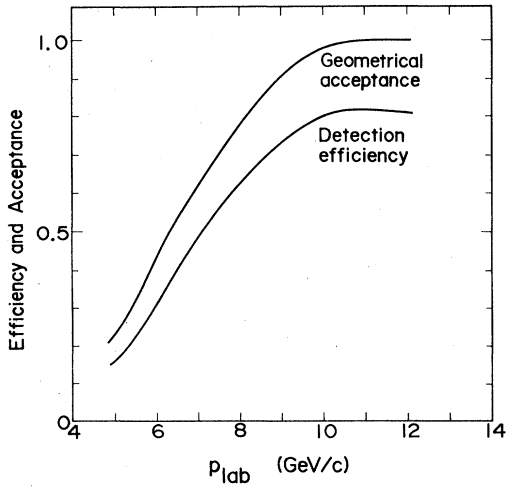

FIG. 3. The detection efficiency and the geometrical acceptance of the Λ^0 detection system.

included the effects due to decay in flight of the π^-, multiple Coulomb scattering, and energy loss. The hit patterns in the chamber planes and the trigger counters were calculated and encoded into binary data of the same format as the real data. The calculation of the hit patterns in the chambers was based on the efficiencies and resolutions of the chambers, which were determined from the real data by the track-finding program.

The Monte Carlo events were processed by the off-line program in the same way as the real data. The geometrical acceptance of the spectrometer was defined as the ratio of the number of $\Lambda^0 \to p\pi^-$ events in which p and π^- were emitted within the geometrical boundary of the spectrometer to the number of $\Lambda^0 \to p\pi^-$ decays which took place in the decay region. The detection efficiency of the spectrometer was defined as the ratio of the number of reconstructed events to that of the $\Lambda^0 \to p\pi^-$ decays. The geometrical acceptance and the detection efficiency are plotted as a function of the Λ^0 momentum in Fig. 3. The geometrical acceptance decreases with the Λ^0 momentum below 10 GeV/c because the pion acceptance of the spectrometer magnet $D1$ decreases at lower momenta.

C. The invariant cross section

In terms of the Λ^0 momentum $p_{\rm lab}$ and the production angle θ in the laboratory, the invariant cross section is given by

$$E\frac{d^3\sigma}{dp^3}=\frac{E_{\rm lab}}{p_{\rm lab}^2}\frac{d^2\sigma}{dp_{\rm lab}d\Omega} \tag{1}$$

with

$$\frac{d^2\sigma}{dp_{\rm lab}d\Omega}=\frac{N_\Lambda(p_{\rm lab},\theta)}{\epsilon_{p\pi}\epsilon_{\rm decay}R_{p\pi}\epsilon_{\rm CPU}N_tN_b\Delta p\,\Delta\Omega}\ . \tag{2}$$

Here $N_\Lambda(p_{\rm lab},\theta)$ is the measured number of $\Lambda^0 \to p\pi^-$ events at a given angle and momentum, Δp is the momentum bin width, which was chosen to be $\Delta p=0.25$ GeV/c, $\Delta\Omega$ is the solid angle determined by the collimator, $\epsilon_{p\pi}$ is the detection efficiency of the spectrometer defined in Sec. III B, $\epsilon_{\rm decay}$ is the probability that the Λ^0 produced at the target decays in the decay region, where the proper mean lifetime of Λ^0 is given by $c\tau=7.89$ cm from Ref. 20, $R_{p\pi}$ is the branching ratio of the $\Lambda^0 \to p\pi^-$ decay (0.642 from Ref. 20), $\epsilon_{\rm CPU}$ is the fractional number of the event triggers that were logged on the raw data tape by the data processor Eclipse, N_t is the number of target nuclei per unit area, and N_b is the number of incident protons which struck the target. In the calculation of $\epsilon_{\rm CPU}$ the number of the triggers was corrected for accidental veto rates by S1, which were at most 10% of the triggers.

D. Corrections

Two corrections were applied to the cross sections obtained in Eq. (2): one is concerned with the absorption in the target and the other is the effective solid angle of the collimator.

Corrections for the absorption were made by comparing the Λ^0 yields from the 20-mm-thick target and the 40-mm-thick target. Let σ_{20} (σ_{40}) be the cross section from the 20-mm- (40-mm-) thick target, and let R represent the ratio σ_{40}/σ_{20}. We assume that the incident protons are absorbed in the target with a mean free path of l_1 and the produced Λ^0's with a mean free path of l_2. Then the cross section σ that is corrected for the absorption is given by

$$\sigma=\sigma_{20}\epsilon_{\rm abs} \tag{3a}$$

with

$$\epsilon_{\rm abs}=(L/l_1-L/l_2)/(e^{-L/l_2}-e^{-L/l_1})\ , \tag{3b}$$

$$l_2=-L/\ln(2R-e^{-L/l_1})\ , \tag{3c}$$

where L is the thickness of the 20-mm-thick target. The calculation of the l_2 and the correction factor $\epsilon_{\rm abs}$ was made by substituting the interaction length[20] of protons for the l_1. Since the measured values of R turned out to be essentially independent of the Λ^0 momentum, we assumed that the absorption correction was independent of the momentum in the present experiment. The results are listed in Table II.

The mean free path of Λ^0's, l_2, obtained in the above procedure, coincided with the collision length[20] of protons rather than the interaction length[20] of protons, as shown in Table II. If we assume that the collision length of Λ^0's is equal to that of protons,[21] then the above result implies that elastic scattering as well as inelastic scattering lead to the absorption of Λ^0's in the target. This is reasonable, since Λ^0's which are scattered elastically in the target will have little chance to pass through the collimator, and hence most of them will not be detected.

The effective solid angle of the collimator was evaluated by taking into account the scattering and absorption of Λ^0's in the collimator and the finite spread of the production points of Λ^0's in the target. The collision length of Λ^0's was assumed to be the same as that of protons, and the (x_F,p_T) distribution in Λ^0-nucleus scattering was approximated by that[22] in the $p+p \to p+X$ reaction. The scattering and finite absorption of Λ^0's increased the ef-

TABLE II. Parameters of the target absorption. Here R ($=\sigma_{40}/\sigma_{20}$) is the measured ratio of the Λ^0 yields from the 40-mm-thick target to that from the 20-mm-thick target, and l_1 is the absorption length of protons (Ref. 20); the mean free path of Λ^0's, l_2, and the correction factor $\epsilon_{\rm abs}$ were calculated from R and l_1 (see the text); l_c is the collision length of protons (Ref. 20).

Target material	R	l_1 (cm)	l_2 (cm)	$\epsilon_{\rm abs}$	l_c (cm)
Be	0.941±0.02	36.7	30±2	1.063±0.003	30.0
Cu	0.853±0.01	14.8	11±2	1.17 ±0.02	9.3
W	0.769±0.01	10.3	6.0±0.6	1.30 ±0.02	5.6

fective solid angle by 12% of the geometrical solid angle, while the finite spread of the Λ^0 production points decreased it by 3%. Therefore, the effective solid angle was determined to be 109 μsr.

In the above context we note that the scattering of Λ^0's in the collimator also brings about a shift in the momentum spectra of Λ^0's. This effect was evaluated in a similar way, and it turned out that the amount of corrections in the measured momentum spectra of Λ^0's was 3% at lower momenta and less than 1% at higher momenta.

E. Estimation of systematic errors

The errors quoted in the tables and figures of this paper are statistical only. The major systematic error in the present measurement is the overall uncertainty in the normalization of the cross sections. This is composed of the uncertainty in the absolute intensity calibration of the primary protons (15%), that in the collimator solid angle (5%), and that in the detection efficiency for the $\Lambda^0 \rightarrow p\pi^-$ decay (5%). The uncertainty in the Λ^0 detection efficiency was mainly due to the uncertainty in the estimation of the chamber efficiencies. Adding these uncertainties in quadrature, we estimated the overall normalization uncertainty to be 20%.

Another systematic error is due to fluctuation of the beam conditions, which introduces the target-to-target and angle-to-angle errors. This error was estimated to be less than 7% from examination of the run-to-run reproducibility of the Λ^0 yield.

IV. RESULTS AND DISCUSSION

A. The invariant cross sections

Figures 4(a)—4(c) show the invariant cross sections as a function of the Λ^0 momentum $p_{\rm lab}$ at the three production angles. The curves are drawn to guide the eye.

It is convenient to express the invariant cross sections as a function of the Feynman scaling variable x_F and the transverse momentum p_T of the Λ^0. The x_F is defined as $x_F = p_L^* / p_{\rm max}^*$, where p_L^* and $p_{\rm max}^*$ are, respectively, the longitudinal momentum of the Λ^0 and its kinematic limit in the center-of-mass frame of the incident proton and the target. Values of x_F were calculated under the assumption that the target was a free proton. Under this assumption, $p_{\rm max}^*$ is 2.2 GeV/c for the incident proton energy of 12 GeV. We note that, given the production angle θ, the x_F and the p_T are not independent variables but are mutually related. The invariant cross sections as a function of x_F and p_T were obtained by binning the data into x_F bins at intervals of 0.1 at each angle θ, with the corresponding value of p_T being calculated from the x_F and θ. The results are summarized in Table III.

B. The A dependence

The A dependence of the invariant cross sections expressed as a function of x_F and p_T was analyzed under the power-law hypothesis:

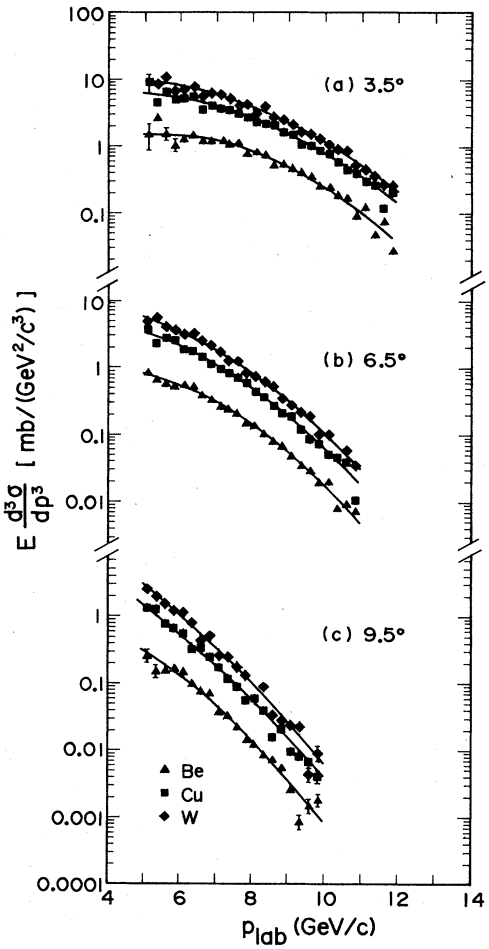

FIG. 4. Invariant cross sections as a function of $p_{\rm lab}$ at (a) 3.5°, (b) 6.5°, and (c) 9.5°. The curves are drawn to guide the eye.

$$E\frac{d^3\sigma}{dp^3}(x_F,p_T,A)=E\frac{d^3\sigma}{dp^3}(x_F,p_T,A=1)A^{\alpha(x_F,p_T)} . \quad (4)$$

Figure 5 shows several of the invariant cross sections versus the atomic mass A on a log-log plot, together with the fitted lines. This demonstrates that our results are consistent with the power-law fit. Extrapolation of the cross sections off nuclei to $A=1$ according to Eq. (4) yields the cross section for $A=1$, $E\,d^3\sigma/dp^3(x_F,p_T, A=1)$.

The exponent $\alpha(x_F,p_T)$ that was obtained in Eq. (4) is listed in Table IV, and is plotted versus p_T for each bin of x_F in Fig. 6. Also shown are the data[2] at 300 GeV for comparison. The $\alpha(x_F,p_T)$ at 12 GeV agrees fairly well with that at 300 GeV, and shows a tendency to increase with increasing p_T. The observed agreement of $\alpha(x_F,p_T)$ between 12 and 300 GeV implies that nuclear effects in Λ^0 production by protons off nuclei are essentially the same in the energy range considered.

The model of Dar and Takagi[7] describes hadron production from nuclei at the beam-fragmentation region by taking into account quark attenuation in nuclear matter in the framework of the constituent-quark model, and gives the prediction of $\alpha(x_F,p_T=0)$. In order to compare our

TABLE III. The invariant cross sections as a function of x_F and p_T. The errors are statistical only, and do not include the overall normalization uncertainty of 20%.

x_F	p_T (GeV/c)	$E\,d^3\sigma/dp^3$ [mb/(GeV^2/c^3)] Be	Cu	W
$\theta=3.5°$				
0.35	0.34	1.79 ±0.16	5.9 ±0.4	8.9 ±0.6
0.45	0.40	1.33 ±0.06	4.51 ±0.15	6.7 ±0.2
0.55	0.47	1.01 ±0.03	3.14 ±0.07	4.62 ±0.11
0.65	0.53	0.607 ±0.015	1.90 ±0.03	2.88 ±0.06
0.75	0.60	0.318 ±0.008	0.949 ±0.018	1.39 ±0.03
0.85	0.66	0.132 ±0.004	0.404 ±0.010	0.628 ±0.016
$\theta=6.5°$				
0.25	0.56	0.73 ±0.07	3.27 ±0.18	5.3 ±0.4
0.35	0.68	0.58 ±0.02	2.28 ±0.06	3.58 ±0.12
0.45	0.80	0.316 ±0.008	1.092 ±0.019	1.94 ±0.04
0.55	0.92	0.137 ±0.003	0.491 ±0.008	0.799 ±0.016
0.65	1.05	0.0467 ±0.0012	0.157 ±0.003	0.274 ±0.006
0.75	1.18	0.0126 ±0.0005	0.0445±0.0012	0.072 ±0.003
$\theta=9.5°$				
0.25	0.90	0.202 ±0.015	1.01 ±0.06	2.03 ±0.10
0.35	1.09	0.090 ±0.004	0.351 ±0.013	0.66 ±0.02
0.45	1.29	0.0204 ±0.0011	0.084 ±0.003	0.164 ±0.006
0.55	1.49	0.0044 ±0.0003	0.0158±0.0009	0.0300±0.0018
0.65	1.71	0.00073±0.00010	0.0033±0.0003	0.0045±0.0005

data with the model prediction, the values of $\alpha(x_F,p_T=0)$ were obtained by extrapolating the data points linearly to $p_T=0$ at each bin of x_F. The obtained $\alpha(x_F,p_T=0)$ is plotted versus x_F in Fig. 7. Also shown are the data[2] at 300 GeV and the prediction[7] of the constituent-quark model. In view of possible errors associated with the linear extrapolation of the data points to $p_T=0$, our results are consistent with the model prediction.

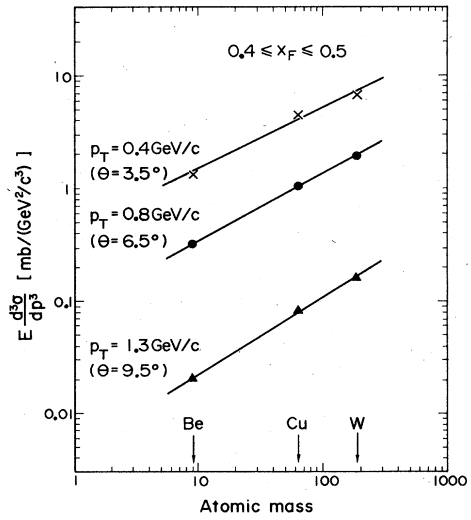

FIG. 5. Invariant cross sections as a function of the target mass number A at $0.4\leq x_F\leq 0.5$. The straight lines are the power-law fit.

C. Feynman scaling

As mentioned in Sec. I, the Feynman scaling for Λ^0 production has been studied with bubble chambers in terms of the invariant cross sections integrated over p_T.[1] We are now in a position to compare the data as a function of (x_F,p_T) between 12 and 300 GeV. We plot in Figs. 8(a)—8(c) the invariant cross sections for $A=1$ (extrapolated), Be, Cu, and W at 12 GeV as a function of p_T at three typical bins of x_F, together with the data[2] for $A=1$ (extrapolated) and Be by 300-GeV protons. The figures show that the cross sections at 12 GeV are smaller than the cross sections at 300 GeV, particularly at high p_T. This indicates that Λ^0 production by protons does not reach the Feynman scaling limit at 12 GeV in the (x_F,p_T) region covered by this experiment.

TABLE IV. Exponents $\alpha(x_F,p_T)$ of the A dependence are shown as a function of x_F at each production angle. The errors are statistical only.

x_F	$\alpha(x_F,p_T)$ $\theta=3.5°$	$\theta=6.5°$	$\theta=9.5°$
0.25		0.667±0.040	0.761±0.030
0.35	0.532±0.036	0.613±0.017	0.664±0.019
0.45	0.536±0.019	0.604±0.011	0.690±0.022
0.55	0.511±0.012	0.592±0.010	0.640±0.031
0.65	0.520±0.010	0.590±0.012	0.617±0.061
0.75	0.495±0.010	0.587±0.017	
0.85	0.519±0.013		

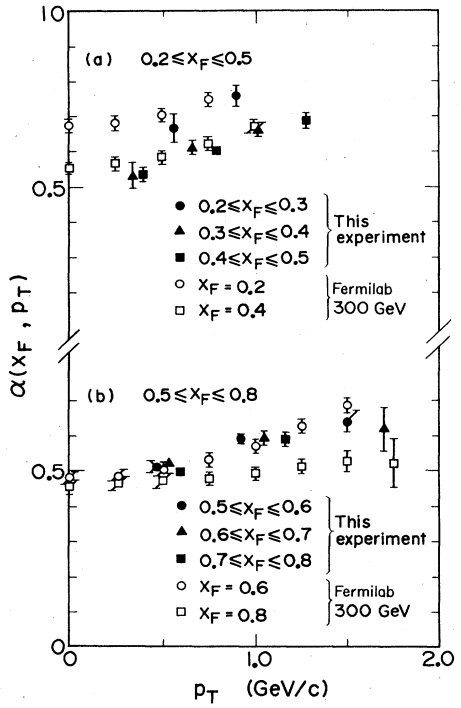

FIG. 6. Exponents $\alpha(x_F,p_T)$ as a function of p_T for (a) $0.2 \leq x_F \leq 0.5$ and (b) $0.5 \leq x_F \leq 0.8$. The data at 300 GeV (Ref. 2) are shown for comparison.

D. The p_T dependence

The p_T dependence of the Λ^0 invariant cross sections was fit to the phenomenological Gaussian form:

$$E\frac{d^3\sigma}{dp^3}(x_F,p_T)=E\frac{d^3\sigma}{dp^3}(x_F,p_T=0)e^{-b(x_F)p_T^2} . \quad (5)$$

Figures 8(a)—8(c) show that gross features of our results are consistent with the Gaussian fit of Eq. (5).

The slope parameters $b(x_F)$ obtained in the Gaussian fit are plotted versus x_F in Fig. 9. Comparison of the

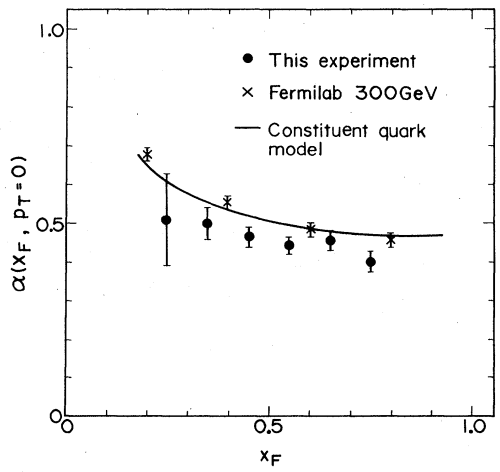

FIG. 7. The x_F dependence of α at $p_T=0$: $\alpha(x_F,p_T=0)$. The data at 300 GeV (Ref. 2) are also shown. The curve is due to the constituent-quark model of Dar and Takagi (Ref. 7).

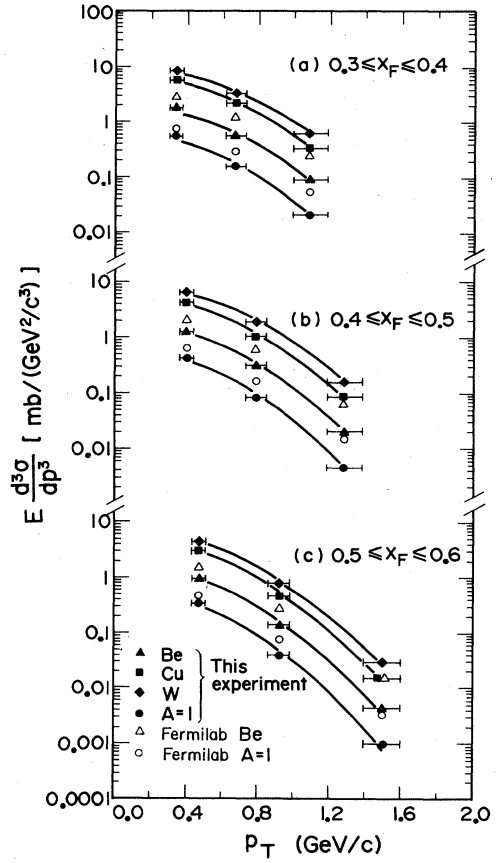

FIG. 8. Invariant cross sections as a function of p_T at (a) $0.3 \leq x_F \leq 0.4$, (b) $0.4 \leq x_F \leq 0.5$, and (c) $0.5 \leq x_F \leq 0.6$. The curves are the Gaussian fit. The data at 300 GeV (Ref. 2) are shown for comparison.

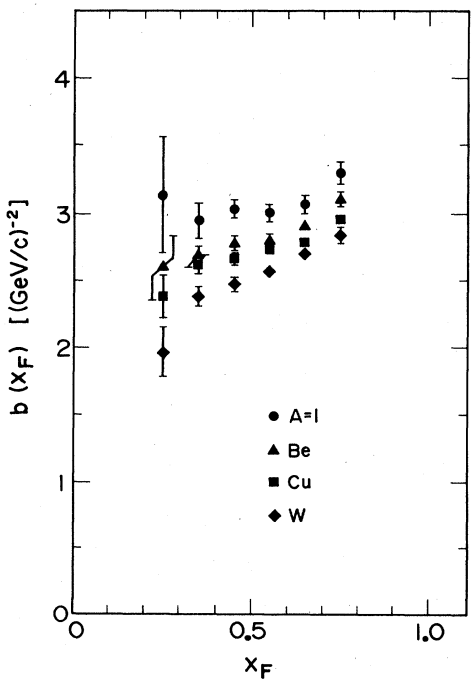

FIG. 9. Slope parameters of the p_T dependence: $b(x_F)$.

$b(x_F)$ for different nuclei at a given x_F shows that the $b(x_F)$ is a decreasing function of the atomic mass A, reflecting the fact that the p_T spectrum at a given x_F becomes broader as the A increases. The x_F dependence of $b(x_F)$ is also A dependent. The $b(x_F)$ for the $A=1$ extrapolated cross section remains approximately constant in the measured range of x_F, while the $b(x_F)$ for nuclear targets decreases with decreasing x_F, the rate of decrease being faster for higher A.

E. Comparison with the triple-Regge model

The triple-Regge model provides a phenomenological description of the high-energy inclusive reactions.[11,12] The limit $s/M^2 \to \infty$ and $M^2 \to \infty$ at fixed t is called the triple-Regge limit, where s is the square of the center-of-mass energy, $s=(p_b+p_t)^2$; t is the square of the four-momentum transfer, $t=(p_b-p_\Lambda)^2$; M^2 is the square of the missing mass, $M^2=(p_b+p_t-p_\Lambda)^2$; and p_b, p_t, and p_Λ are the four-momenta of the incident beam proton, the target proton, and the produced Λ^0, respectively. At this limit, the invariant cross section for Λ^0 production is written as[12]

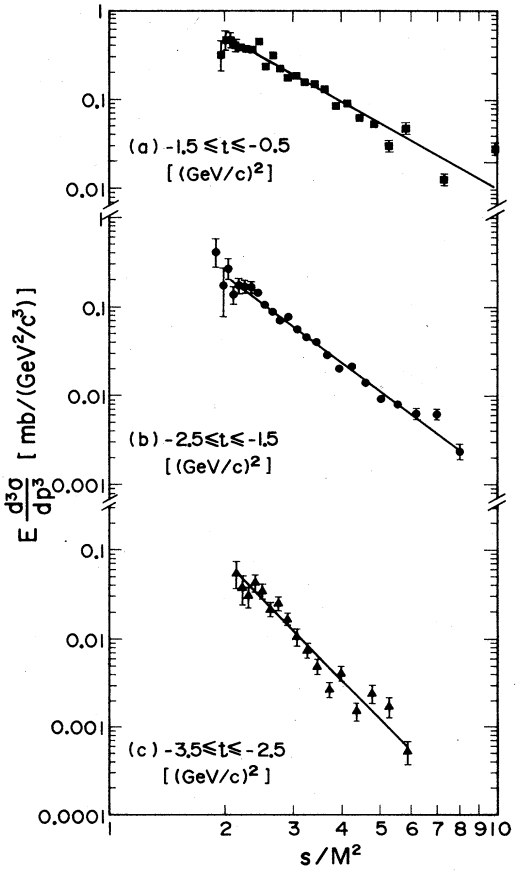

FIG. 10. Invariant cross sections as a function of s/M^2 at (a) $-1.5 \le t \le -0.5$ (GeV/c)^2, (b) $-2.5 \le t \le -1.5$ (GeV/c)^2, and (c) $-3.5 \le t \le -2.5$ (GeV/c)^2. The lines are the triple-Regge fit.

TABLE V. Results of the triple-Regge fit. The $\alpha_R(t)$ is the Regge trajectory and $G(t)$ is the triple-Regge coupling. The χ^2/DF (χ^2 divided by the number of degrees of freedom) are also shown.

t (GeV/c)^2	$\alpha_R(t)$	$G(t)$ [mb/(GeV^2/c^3)]	χ^2/DF
$-3.5 \le t \le -2.5$	-1.75 ± 0.10	1.8 ± 0.4	36/19
$-2.5 \le t \le -1.5$	-1.13 ± 0.04	2.2 ± 0.2	40/22
$-1.5 \le t \le -0.5$	-0.72 ± 0.04	2.8 ± 0.2	109/22

$$E\frac{d^3\sigma}{dp^3}=\frac{1}{\pi}\frac{d^2\sigma}{dt\,d(M^2/s)}=G(t)\left[\frac{s}{M^2}\right]^{2\alpha_R(t)-1}, \quad (6)$$

where $\alpha_R(t)$ is the effective Regge trajectory for the $p\bar{\Lambda}^0$ vertex and $G(t)$ is the triple-Regge coupling.

Comparison with the triple-Regge model was made in the following way. The A dependence of the invariant cross sections expressed as a function of $p_{\rm lab}$ and θ was fit to the power-law hypothesis:

$$E\frac{d^3\sigma}{dp^3}(p_{\rm lab},\theta,A)=E\frac{d^3\sigma}{dp^3}(p_{\rm lab},\theta,A=1)A^{\alpha(p_{\rm lab},\theta)}. \quad (7)$$

The cross sections that were extrapolated to $A=1$ in Eq. (7) were binned into three intervals of t, $-3.5 \le t \le -2.5$ (GeV/c)^2, $-2.5 \le t \le -1.5$ (GeV/c)^2, and $-1.5 \le t \le -0.5$ (GeV/c)^2, and were fit to Eq. (6) within the range $2 \le s/M^2 \le 10$. Our data are consistent with the fit of the triple-Regge model, as shown in Fig. 10. The results of the fit are summarized in Table V.

The obtained trajectory $\alpha_R(t)$ is plotted versus t in Fig. 11. Other previous results are also shown for comparison: the $A=1$ extrapolated data[16] from the counter experiment at 300 GeV (Fermilab) and the data[13–15] from hydrogen-bubble-chamber experiments. Our data agrees with that

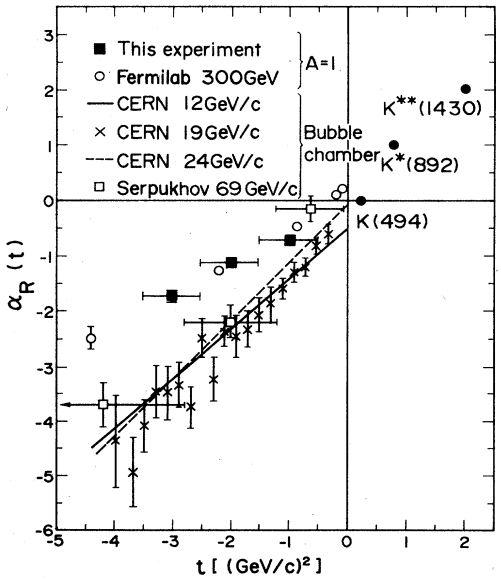

FIG. 11. Regge trajectory $\alpha_R(t)$ in comparison with other experiments: Fermilab 300 GeV (Ref. 16); CERN 12 GeV/c (Ref. 13); CERN 19 GeV/c (Ref. 14); CERN 24 GeV/c (Ref. 13); Serpukhov 69 GeV/c (Ref. 15).

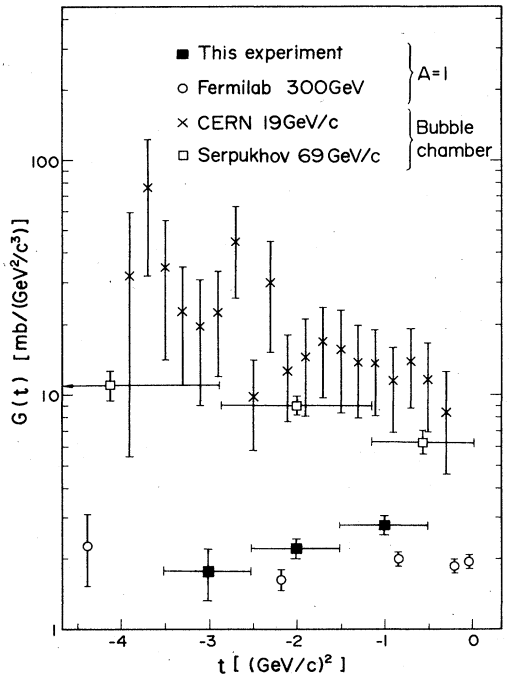

FIG. 12. Triple-Regge coupling $G(t)$ in comparison with other experiments: Fermilab 300 GeV (Ref. 16); CERN 19 GeV/c (Ref. 14); Serpukhov 69 GeV/c (Ref. 15).

of the counter experiment at 300 GeV, both of them lying close to the straight line defined by $K^*(892)$ and $K^{**}(1430)$, while they show a significant disagreement with the bubble-chamber data. The coupling $G(t)$ obtained is plotted in Fig. 12, together with the previous data. Here again, our data agrees with that at 300 GeV but disagrees with the bubble-chamber data. We note in passing that the big difference in $G(t)$ as displayed in Fig. 12 is in effect a reflection of the difference in $\alpha_R(t)$.

Possible explanations of the discrepancy observed between the counter experiments and the bubble-chamber experiments are as follows. (1) The discrepancy may be caused by the difference in the kinematic region. The majority of Λ^0's detected with bubble chambers lies in the central region of the Peyrou plot, while the Λ^0's detected in the counter experiments come from the beam-fragmentation region, where the triple-Regge model is believed to be valid. (2) The discrepancy may originate in the difference in the target materials. Several recent experiments[23] have revealed that the cross sections for inclusive hadron production off nuclei, when extrapolated to $A=1$ by the power-law fit, do not reproduce the cross sections from hydrogen.

The agreement of $\alpha_R(t)$ and $G(t)$ between 12 and 300 GeV implies that the invariant cross sections scale as a function of t and s/M^2. On the other hand, as discussed in Sec. IV C, the scaling of the invariant cross sections as a function of x_F and p_T (the Feynman scaling) does not reach the scaling limit at 12 GeV. These two facts seem to contradict each other, since the triple-Regge model, Eq. (6), yields the Feynman scaling at high energies; i.e., at the limit $s\to\infty$ and $p_L^* \gg p_T$, one gets $M^2/s \to 1-x_F$ and $t\to 2{p_T}^2/x_F$. We note, however, that this approximation is not adequate at 12 GeV. In fact, for given values of s/M^2 and t, the p_T and x_F at 12 GeV are smaller than the corresponding values at 300 GeV, and the invariant cross sections show an increase at lower p_T. Hence, the scaling of the invariant cross sections as a function of s/M^2 and t does not mean the Feynman scaling at 12 GeV.

V. CONCLUSIONS

The invariant cross sections for inclusive Λ^0 production by 12-GeV protons on beryllium, copper, and tungsten were measured at 3.5°, 6.5°, and 9.5°. The kinematic range covered is $0.2 \le x_F \le 0.9$ and $0.35 \le p_T \le 1.7$ GeV/c. The conclusions of this experiment can be summarized as follows.

(1) The A dependence of the invariant cross sections is fit to the power-law hypothesis A^α. The obtained exponent $\alpha(x_F,p_T)$ agrees with that at 300 GeV, and tends to increase as the p_T increases. The exponent $\alpha(x_F,p_T=0)$ that was obtained through an extrapolation to $p_T=0$ is consistent with the prediction of the constituent-quark model, although more precise data are needed to draw a definite conclusion.

(2) Comparison of the invariant cross sections as a function of (x_F,p_T) between 12 and 300 GeV indicates that Λ^0 production by protons does not reach the Feynman-scaling limit at 12 GeV.

(3) The p_T dependence of the invariant cross sections is fit to the Gaussian form $e^{-bp_T^2}$. The A dependence of the slope parameter $b(x_F)$ is observed.

(4) The triple-Regge behavior of the $A=1$ extrapolated cross sections agrees with that obtained in the counter experiment at 300 GeV, while it is significantly different from the results obtained in hydrogen-bubble-chamber experiments.

ACKNOWLEDGMENTS

We would like to thank Professor T. Nishikawa, Professor S. Suwa, Professor S. Ozaki, and Professor A. Kusumegi for their encouragement during the course of the experiment. We wish to thank members of the KEK accelerator division and members of the beam-channel group for their trouble-free operation of the proton beam. We wish also to thank members of the KEK data-handling division for their kind help in the data analysis. We greatly appreciate the patient support of Dr. A. Yamamoto and Professor K. Kondo in the intensity calibration of the primary proton beam. Thanks are due to Professor L. Pondrom for helpful discussions on various aspects of the experiment, and to Dr. F. Takagi for helpful discussions on the A dependence.

*Present address: Department of Physics, Chuo University, Kasuga, Bunkyo-ku, Tokyo 112, Japan.
†Present address: Institute for Nuclear Study, University of Tokyo, Tanashi, Tokyo 188, Japan.
‡Present address: Fermi National Accelerator Laboratory, P.O. Box 500, Batavia, IL 60510.

[1]J. Whitmore, Phys. Rep. **27C**, 187 (1976), and references therein.
[2]K. Heller *et al.*, Phys. Rev. D **16**, 2737 (1977); P. Skubic *et al.*, *ibid.* **18**, 3115 (1978).
[3]F. Dydak *et al.*, Nucl. Phys. **B118**, 1 (1977); F. Lomanno *et al.*, Phys. Rev. Lett. **43**, 1905 (1979).
[4]F. Abe *et al.*, Nucl. Instrum. Methods **220**, 293 (1984).
[5]F. Abe *et al.*, Phys. Rev. Lett. **50**, 1102 (1983); F. Abe *et al.*, J. Phys. Soc. Jpn. **52**, 4107 (1983).
[6]See, for example, reviews by A. Białas, in *Multiparticle Dynamics 1982,* proceedings of the XIIIth International Symposium, Volendam, The Netherlands, edited by E. W. Kittel, W. Metzger, and A. Stergiou (World Scientific, Singapore, 1983), pp. 328—358; W. Busza, in *Proceedings of the II International Symposium on Hadron Structure and Multiparticle Production, Kazimierz, Poland, 1979,* edited by Z. Ajduk (Institute of Theoretical Physics, Warsaw University, Warsaw, 1979), pp. 145—173; C. Halliwell, in *Proceedings of the VIII International Symposium on Multiparticle Dynamics, Kaysersberg, France, 1977,* edited by R. Arnold, J.-P. Gerber, and P. Schübelin (Centre de Recherches Nucleaires, Strasbourg, France, 1977), pp. D1—D56.
[7]A. Dar and F. Takagi, Phys. Rev. Lett. **44**, 768 (1980).
[8]N. N. Nikolaev and S. Pokorski, Phys. Lett. **80B**, 290 (1979); B. Durand and J. Krebs, Phys. Rev. D **21**, 3137 (1980).
[9]R. P. Feynman, Phys. Rev. Lett. **23**, 1415 (1969).
[10]M. L. Perl, *High Energy Hadron Physics* (Wiley, New York, 1974), pp. 186—192; H. Bøggild and T. Ferbel, Annu. Rev. Nucl. Sci. **24**, 451 (1974).
[11]A. H. Mueller, Phys. Rev. D **2**, 2963 (1970); C. E. DeTar *et al.*, Phys. Rev. Lett. **26**, 675 (1971).
[12]S. N. Ganguli and D. P. Roy, Phys. Rep. **67C**, 201 (1980).
[13]V. Blobel *et al.*, Nucl. Phys. **B135**, 379 (1978).
[14]K. Alpgård *et al.*, Nucl. Phys. **B105**, 349 (1976).
[15]H. Blumenfeld *et al.*, Nucl. Phys. **B125**, 253 (1977).
[16]T. Devlin *et al.*, Nucl. Phys. **B123**, 1 (1977).
[17]A. Yamamoto, KEK Report No. 81-13, 1981 (unpublished).
[18]S. Dhawan, IEEE Trans. Nucl. Sci. **NS-21**, 922 (1974); S. Dhawan *et al.*, Jpn. J. Appl. Phys. **23**, 492 (1984).
[19]H. Hirabayashi *et al.*, J. Phys. Soc. Jpn. **51**, 3098 (1982).
[20]R. L. Kelly *et al.* (Particle Data Group), Rev. Mod. Phys. **52**, S1 (1980).
[21]This assumption is not unreasonable, since the total cross section for $\Lambda^0 p$ collisions is observed to be approximately 90% of the total cross section for pp collisions at the momentum region from 6 to 21 GeV/c; see S. Gjesdal *et al.*, Phys. Lett. **40B**, 152 (1972).
[22]J. Whitmore *et al.*, Phys. Rev. D **11**, 3124 (1975).
[23]L. Kluberg *et al.*, Phys. Rev. Lett. **38**, 670 (1977); D. Antreasyan *et al.*, Phys. Rev. D **19**, 764 (1979); B. Brown *et al.*, Phys. Rev. Lett. **50**, 11 (1983); D. S. Barton *et al.*, Phys. Rev. D **27**, 2580 (1983).